Nanostructuring Pt-Pd Bimetallic Electrocatalysts for CO_2 Reduction Using Atmospheric Pressure Atomic Layer Deposition

Li, Ming; Fu, Shilong; Saedy, Saeed; Rajendrakumar, Aparna; Tichelaar, Frans D.; Kortlever, Ruud; van Ommen, J. Ruud

DOI
10.1002/cctc.202200949

Publication date
2022

Document Version
Final published version

Published in
ChemCatChem

ChemCatChem

Research Article
doi.org/10.1002/cctc.202200949

Chemistry Europe
European Chemical Societies Publishing

www.chemcatchem.org

Nanostructuring Pt-Pd Bimetallic Electrocatalysts for CO_2 Reduction Using Atmospheric Pressure Atomic Layer Deposition

Ming Li,[a, b] Shilong Fu,[b] Saeed Saedy,*[a] Aparna Rajendrakumar,[a] Frans D. Tichelaar,[c] Ruud Kortlever,*[b] and J. Ruud van Ommen[a]

Preparing supported nanoparticles with a well-defined structure, uniform particle size, and composition using conventional catalyst synthesis methods, such as impregnation, precipitation, and deposition-precipitation is challenging. Furthermore, these liquid phase methods require significant solvent consumption, which has sustainable issues and requires complex purification processes, usually leaving impurities on the catalyst, affecting its selectivity and activity. In this work, we employed atomic layer deposition (ALD, a vapor phase synthesis method) to synthesize electrocatalysts with well-controlled core-shell and alloy structures for CO_2 reduction to formic acid. With this approach, the structural control of the catalysts is down to the atomic scale, and the effect of core-shell and alloy structure on Pt–Pd bimetallic catalysts has been investigated. It is shown that the Pt–Pd alloy catalyst displays a 46% faradaic efficiency toward formic acid, outperforming Pt@Pd and Pd@Pt core-shell structures that show faradaic efficiencies of 22% and 11%, respectively. Moreover, both core-shell bimetallic catalysts (Pd@Pt and Pt@Pd) are not stable under electroreduction conditions. These catalysts restructure to more thermodynamically stable structures, such as segregated clusters or alloy particles, during the electrochemical reduction reaction, altering the catalytic selectivity.

Introduction

The electrochemical reduction of CO_2 provides an attractive pathway to convert waste CO_2 with water and renewable electricity into chemicals or fuels.[1] It can thereby provide a way to store intermittent electricity in the form of chemical bonds and aid in the defossilization of the chemical industry, paving the way for a carbon-neutral economy. Among the currently available catalysts and targeted products, the commercialization of electrochemically produced formic acid is profitable in comparison with other options.[2] Formic acid is a suitable energy storage medium, and the two-electron pathway for formic acid production requires much less energy input compared to the multi-electron pathways that generate more complex products.[3] However, the most commonly reported catalysts for reducing CO_2 to formic acid, such as In, Sn, Bi, and Pb, suffer from very high overpotentials of more than 1 V or stability issues.[4] The activity and selectivity of a catalyst strongly depend on the particle size, shape, and structural uniformity of these particles.[5] The conventional catalyst synthesis methods, such as impregnation, precipitation, deposition-precipitation and sol-gel, usually fail to control these structural properties well.[6] Moreover, these methods typically require significant amounts of solvent, which generally leave impurities and contaminate the catalyst, affecting its selectivity and activity. Synthesis of catalysts using vapor phase methods offers a viable solution for these issues. The possibility of large-scale production using gas phase methods also promises scalable production of microstructurally well-controlled catalysts.

Various approaches have been proposed to electrochemically reduce CO_2 to formic acid. For example, Zhao et al. reported an electrodeposited Sn electrode that gives a 91% faradaic efficiency for formic acid production at −1.4 V vs. saturated calomel electrode (SCE).[7] A bulk In electrode can reach a faradaic efficiency of ~95% at −1.06 V vs. reversible

[a] M. Li, Dr. S. Saedy, A. Rajendrakumar, Prof. J. R. van Ommen
Chemical Engineering Department
Faculty of Applied Sciences
Delft University of Technology
Van der Maasweg 9
2628 HZ Delft (The Netherlands)
E-mail: S.Saedy@tudelft.nl
[b] M. Li, S. Fu, Dr. R. Kortlever
Process & Energy Department
Faculty of Mechanical
Maritime and Materials Engineering
Delft University of Technology
Leeghwaterstraat 39
2628 CB Delft (The Netherlands)
E-mail: R.Kortlever@tudelft.nl
[c] Dr. F. D. Tichelaar
Quantum Nanoscience Department
Faculty of Applied Sciences
Delft University of Technology
Lorentzweg 1
2628CJ, Delft (The Netherlands)

Supporting information for this article is available on the WWW under https://doi.org/10.1002/cctc.202200949

This publication is part of a joint Special Collection with EurJOC and EurJIC on the Netherlands Institute for Catalysis Research. Please see our homepage for more articles in the collection.

hydrogen electrode (RHE) for the conversion of CO_2 to formic acid.[8] Metallic Pd has been shown to reduce CO_2 to formic acid with low overpotentials and high selectivity.[9] Nevertheless, it is easily poisoned by CO produced during the reaction. Chatterjee and co-workers designed nanoporous Pd alloy electrocatalysts, np-PdX (X = Ag, Cu, Ni, Co), and studied the deactivation process of the electrodes.[10] Pt–Pd bimetallic electrocatalysts have been reported as a promising candidate for this process.[11] This is based on the theory that for a two-electron transfer reaction, the catalyst should be able to catalyze both the forward and reverse reactions.[12] Pt–Pd bimetallic electrocatalysts have been proven to be reputable catalysts for formic acid electro-oxidation. Therefore, they should also be suitable catalysts for the reverse reaction, the electrochemical synthesis of formic acid.[13] Previous studies have established that electrodeposited palladium on a platinum electrode is capable of reducing CO_2 to formic acid from −0.05 V vs. RHE.[13] Furthermore, Pt–Pd bimetallic nanoparticles can reduce CO_2 to formic acid at 0 V vs. RHE and reach a faradaic efficiency of 88% at −0.4 V vs. RHE. The optimized Pd:Pt ratio for this bimetallic electrocatalyst was found to be 7:3 for CO_2 reduction purposes.[11]

All of the previously mentioned studies provide a good foundation to study Pt–Pd bimetallic electrocatalysts for the electroreduction of CO_2 to formic acid. However, none of the previously mentioned studies have investigated the effect of the morphology of Pt–Pd bimetallic structures on its electrocatalytic performance. Atomic layer deposition (ALD), a vapor phase synthesis technique, provides atomic-scale precision in deposition, thereby offering a good opportunity to study the structure effect on catalysts without the influence of other factors.[14] Here, we demonstrate the ability of ALD to make bimetallic electrocatalysts with nano precision control over the morphology. We synthesize well-controlled Pt–Pd electrocatalysts on carbon black support with core-shell and alloy structures using atmospheric pressure ALD.[15] These Pt–Pd structures were subsequently tested for their electrocatalytic properties toward CO_2 reduction to formate.

Results and Discussion

Component and Microstructure Characterization

First, the Pt and Pd ALD growth behavior was studied in a custom-built vibrated fluidized bed reactor operated at atmospheric pressure.[15] 0.5 gram of carbon black was used as substrate in all experiments conducted. Figure S1a shows the saturation behavior of the trimethyl(methylcyclopentadienyl) platinum(IV) ($MeCpPtMe_3$) precursor on carbon black substrate. The Pt content in the samples increases with $MeCpPtMe_3$ dosing time and reaches a plateau after 12 minutes. This indicates that the $MeCpPtMe_3$ precursor reaches self-limiting adsorption on the surface of the substrate. When considering the growth rate of Pt ALD, we found that it reaches a substrate-enhanced growth behavior. After the first cycles of deposition, an average increase of 1.1 wt% per cycle is observed with an increase in cycle numbers (Figure S1b). For Pd deposition, in contrast, the gradual saturation of the formalin co-reactant can be observed in Figure S2a. After 3 minutes of formalin dosing, the Pd content reaches a plateau. This means that the self-limiting phenomena is observed in the formalin dosing curve. However, when it comes to the palladium(II) hexafluoroacetylacetonate ($Pd(hfac)_2$) dosing curve (Figure S2b), no saturation behavior is observed, not even after 30 minutes of continuous $Pd(hfac)_2$ dosing. This observation is in agreement with Liang et al.,[16] who observed that the Pd particle size continues to grow when overdosing the precursor, especially for high specific surface area substrates.[16] It appears that the atomic layer deposition, in this case, has a significant chemical vapor deposition (CVD) component. The growth per cycle (GPC) of Pd deposition was found to be 0.41 wt% per cycle in this study (Figure S2c). Both Pt and Pd depositions showed constant GPC after the first atomic layer deposition cycle.

We synthesized three different Pt–Pd bimetallic catalysts via ALD with a well-defined structure to investigate the nanostructure effects on the electrocatalytic performance for CO_2 electroreduction: a Pt@Pd core-shell, a Pd@Pt core-shell, and a Pt–Pd alloy. As can be seen from Figure 1, Pt–Pd bimetallic nanoparticles of all three morphologies can be clearly seen on the surface of the carbon black substrate. They show comparable particle size distributions and an average particle size of around 8.6 nm. The metal loading and Pd:Pt ratio of these bimetallic samples were determined by inductively coupled plasma-optical emission spectrometry (ICP-OES) and can be found in Table S1. The overall metal loading of all these samples is around 6.7 wt%, and their Pd:Pt ratio are all roughly 65:35. This similarity in particle size and chemical composition helps to exclude the particle size and metal loading effects on the performance of the catalysts with different structure and maintains a single variable in this work. Powder X-ray diffraction (XRD) was conducted to study the crystallinity of these three Pt–Pd bimetallic catalysts. The observed diffraction peaks in Figure 2 can be indexed as (111), (200), (220), and (221) reflections of the fcc structure of Pt and Pd. The peak position of the (111) planes of pure Pt and Pd are located at 39.8° and 40.2°, respectively.[7] For Pt@Pd, the peak corresponding to the (111) plane is shifted to 39.8°, while for Pd@Pt it is shifted to 40.4° and for Pt–Pd alloy it is shifted to 40.1°. This peak position shift indicates lattice distortion in these samples, suggesting that the different nanostructures lead to minor variations in lattice spacing of Pt–Pd bimetallic catalysts.[17] Additionally, the defects and nano-size effects also contribute to this peak shift.

In Figure 3 and Figure S3, the structure of the Pt@Pd and Pd@Pt core-shell nanoparticles, and Pt–Pd alloy are investigated using scanning transmission electron microscopy energy-dispersive X-ray elemental mapping (STEM-EDX mapping) and line-scanning EDX. From Figure 3d, we can see that the Pt particles are encapsulated in a Pd shell, as the Pt@Pd core-shell structure is formed via sequential Pt deposition and Pd deposition. It can also be observed that extremely small Pt particles and slightly larger Pd particles are occasionally present in the samples. Considering their proportion in the sample, their contribution to the CO_2 reduction performance is assumed to

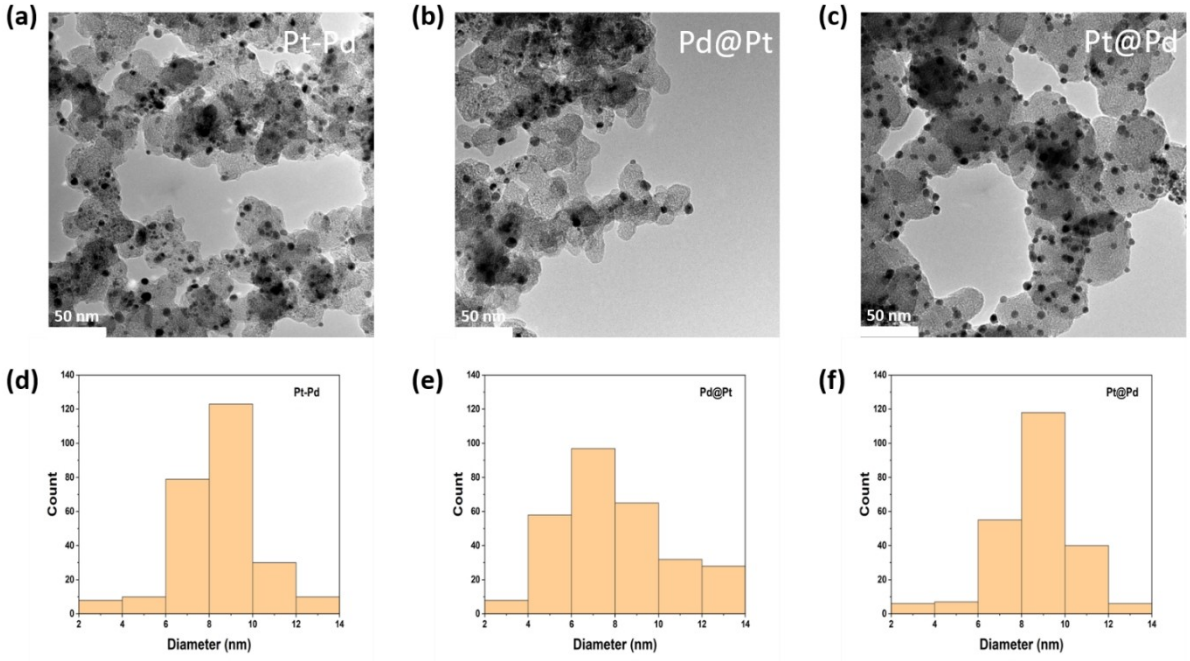

Figure 1. TEM images and particle size distribution of Pt–Pd alloy (a and d), Pd@Pt core-shell (b and e), and Pt@Pd core-shell (c and f) catalysts.

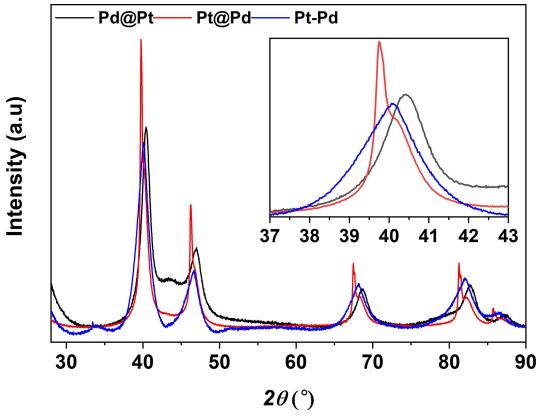

Figure 2. X-ray diffraction patterns of Pt@Pd core-shell, Pd@Pt core-shell, and Pt–Pd alloy catalysts. The inset shows the position of (111) diffraction peak.

be negligible. The line-scanning EDX profile also confirms the Pt@Pd core-shell structure (Figure. S3). A similar core-shell structure can be seen for Pd@Pt sample in Figure 3 (e–h). The corresponding line-scanning EDX profile in Figure S3 also demonstrates the Pd core encapsulated in the Pt shell. On the other hand, Figure 3 (i–l) reveals a random distribution of Pt and Pd for the Pt–Pd alloy sample, implying a random alloy structure in this sample.

X-ray photoelectron spectroscopy (XPS) of the ALD prepared Pt–Pd bimetallic electrocatalysts was carried out to investigate their surface chemistry. The Pt 4f high-resolution spectra suggest that Pt exists in the studied samples in three oxidation states of Pt^0, Pt^{2+}, and Pt^{4+} (Figure 4a–c). The Pt 4f 7/2 peaks are shifted to lower binding energies than pure Pt samples.[18] On the other hand, the Pd 3d spectra indicate that Pd exists in metallic and Pd^{2+} states in the Pt–Pd samples (Figure 4d–f). As demonstrated in Figure 4, a considerable amount of Pt and Pd is oxidized to some degree since the catalysts were synthesized in an oxidative environment. The refined Pd 3d spectra indicate that these peaks are shifted to higher binding energies than pure Pd.[19] For example, the 4f 7/2 peak attributed to Pt^{2+} of the Pt@Pd sample is shifted from 72.7 eV to 72.0 eV, and the Pt^{4+} peak is shifted from 74.9 eV to 73.2 eV.[20] On the other hand, the 3d 5/2 peak corresponding to Pd^0 is shifted from 335.4 eV to 335.6 eV, and the binding energy of Pd^{2+} shifted from 336.4 eV to 336.9 eV. The variation of different peak positions is different for each structure; however, in general, Pt 4f peaks are shifted to lower binding energies, and Pd 3d peaks are shifted to higher binding energies. The negative binding energy shift of Pt and positive binding energy shift of Pd suggest electron transfer from Pd to Pt due to Pd–Pt interactions, altering the electronic structure of Pt–Pd nanoparticles.

Electrochemical Properties

The electrocatalytic performance of Pt–Pd bimetallic electrocatalysts for CO_2 reduction was investigated in a three-electrode electrochemical H-cell at room temperature, where a cation-exchange Nafion 117 membrane separates the anode and cathode compartments. As shown in Figure 5, the Pt–Pd catalyst with the alloy structure displays a better formate faradaic efficiency than the two core-shell catalysts. Moreover,

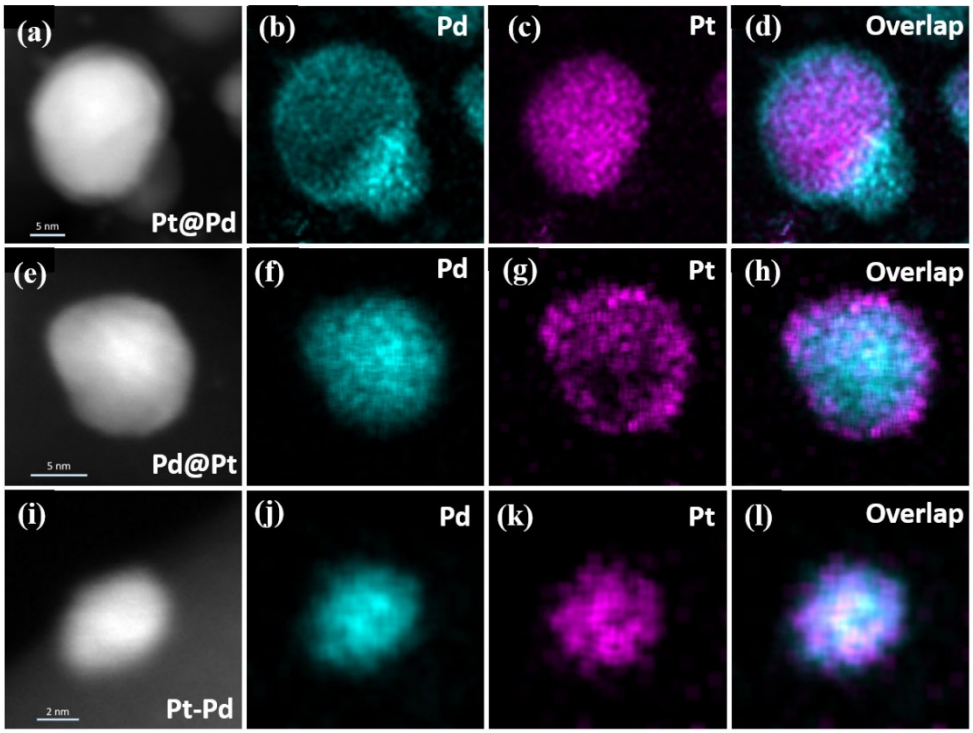

Figure 3. STEM-EDX elemental mappings of the Pt@Pd core-shell (a-d), Pd@Pt core-shell (e-h), and Pt–Pd alloy structure catalysts (i-l).

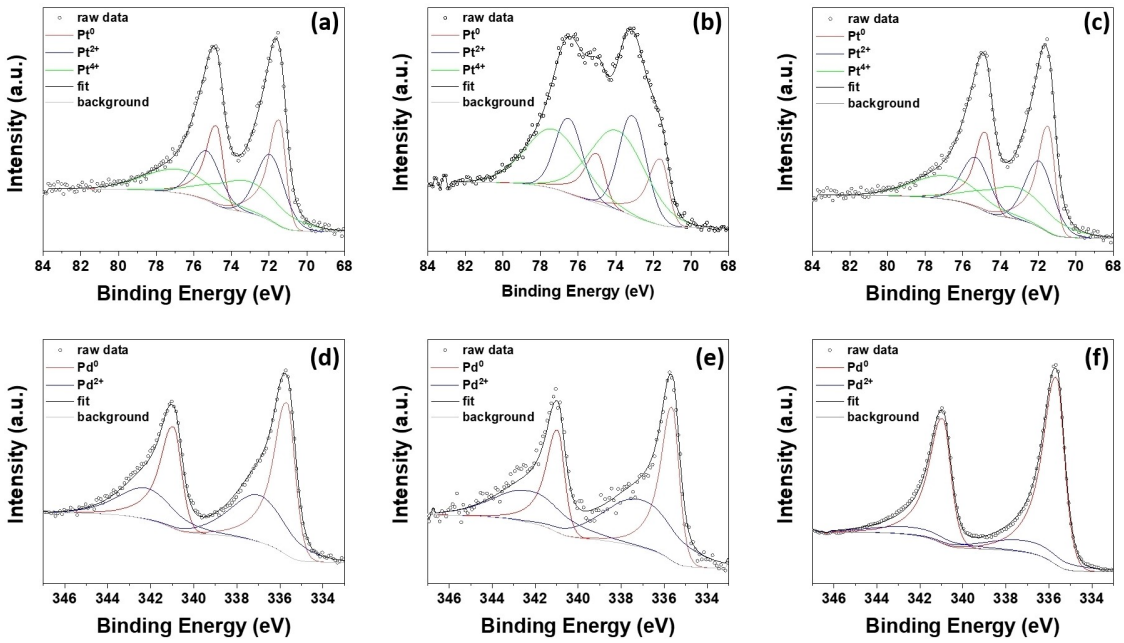

Figure 4. XPS spectra of the Pt@Pd core-shell (a,d), Pd@Pt core-shell (b,e), and Pt–Pd alloy (c,f) catalysts.

the Pt@Pd core-shell catalyst shows a higher formate faradaic efficiency than the Pd@Pt core-shell structure catalysts. We observed that at −0.2 V vs. RHE, a maximum faradaic efficiency of 46% (averaged over one hour) toward formate was achieved for the Pt–Pd alloy catalysts. However, when the applied potential is higher than −0.38 V vs. RHE, the formate faradaic efficiency decreases drastically. We also observed a trend for the Pt–Pd alloy structure catalyst, where the faradaic efficiency of formate increases in the first half hour and then decreases afterward. This suggests that the Pt–Pd alloy nanoparticles are restructuring during the process, which increases the formate selectivity for a while and, in the end, leads to catalyst

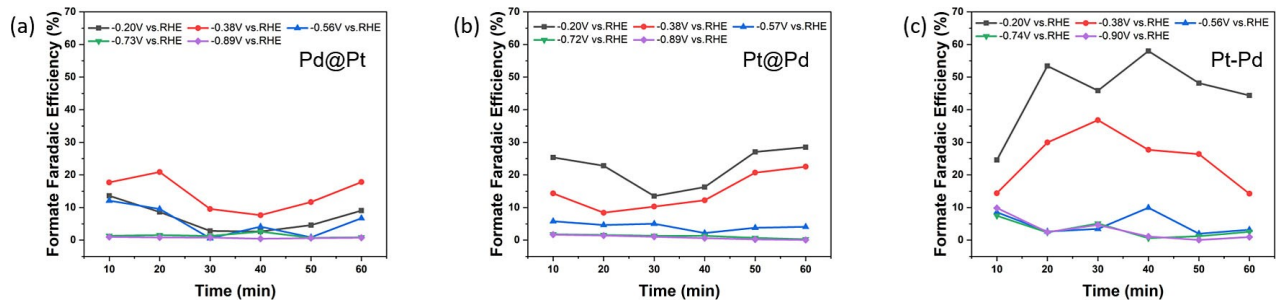

Figure 5. The faradaic efficiency for formate as a function of time at different applied potentials for the a) Pd@Pt core-shell, b) Pt@Pd core-shell, and c) Pt–Pd alloy structure catalysts.

deactivation. When it comes to the core-shell structure catalysts, we found that the Pt@Pd catalysts can achieve 22% (averaged over one hour) FE towards formate at −0.2 V vs. RHE. However, the Pd@Pt catalysts only achieve 7% faradaic efficiency (averaged over one hour) towards formate at −0.2 V vs. RHE and reach a 14% faradaic efficiency (averaged over one hour) towards formate at −0.38 V vs. RHE. The slightly higher formate selectivity of the Pt@Pd sample probably stems from its Pd shell since Pd has higher formate selectivity than Pt. The Pt@Pd and Pd@Pt core-shell catalysts have comparable average particle size and metal loading, so this indicates that adjusting the core-shell metal composition of the core-shell structure catalyst can significantly tune the selectivity of the catalysts. The Pt–Pd bimetallic catalyst prepared by ALD or wet chemistry methods can achieve optimal faradaic efficiencies at different potentials. For example: the Pt–Pd nanoparticles prepared by Kortlever et al.[11] via a co-precipitation method reach an optimal faradaic efficiency at −0.5 V vs. RHE, whilst the catalyst prepared by ALD (this study), reach the highest faradaic efficiency at a much lower overpotential. Diercks et al.[21] report that unsupported PdPt aerogels synthesized by a sol-gel method can reach higher faradaic efficiencies by increasing the Pd content. However, since the amount of binder and the catalyst preparation method are both very different from this work, it is hard to make a comparison between the two catalysts. Since the binder has a significant influence on the catalyst performance,[22] a fair comparison of the effect of synthesis methods on the electrocatalytic performance remains challenging.

Our other observations for the core-shell structured catalysts suggest that their faradaic efficiencies show a trend to decrease in the first half hour and then increase in the following half hour. This is at variance with the trend shown by the catalysts with an alloy structure. This trend lead us to focus on the structure of the catalysts after being used. We performed a STEM-EDX mapping analysis of the catalysts after electrochemistry tests and, as can be seen in Figure S4, we found that the core-shell nanoparticles gradually lost their core-shell structures and formed alloy particles. Similarly, the alloy catalyst became more homogeneous after electrochemistry tests. The instability of the core-shell structured catalysts under the applied potentials explains the trends we observed in Figure 5. It indicates that the alloy structure is more favorable than the core-shell structures for the Pt–Pd bimetallic systems when used as an electrocatalyst for CO_2 reduction. Additionally, the core-shell structures seem unstable and gradually restructure to an alloy phase under the applied potential.

In summary, a way of synthesizing well-controlled core-shell and alloy structured catalysts by ALD on the surface of powder substrate material has been demonstrated. This method is easily scalable to produce large amounts of catalyst and can be used to synthesize other core-shell/alloy structure catalysts for customized applications. Different catalyst structures with a controlled metal loading and particle size can be achieved by changing the deposition sequence and the number of cycles during the ALD process.

Conclusion

Here, Pt–Pd bimetallic catalysts with three different structures have been synthesized, and the effects of the structure of the catalyst nanoparticles on electrocatalytic selectivity for CO_2 reduction to formate have been determined. We find that by controlling the particle size and bimetallic composition, individually changing the structure of the catalyst can have a significant impact on the selectivity. The Pt–Pd alloy catalysts have better selectivity toward formate production than the core-shell structures. Overall, the Pt–Pd alloy catalysts can reach 46% faradaic efficiency at −0.2 V vs. RHE over the course of one hour. The Pd@Pt core-shell structures have lower faradaic efficiencies of 22% and 11%, respectively, at −0.2 V vs. RHE. In addition, we find that the core-shell structures are not stable under electroreduction conditions, irrespective of whether Pd or Pt is the core. During the CO_2 reduction reaction the core-shell catalyst nanoparticles restructure to a thermodynamically more stable alloy form, enhancing their catalytic performance. This re-emphasizes the influence of the catalyst nanostructure on catalyst performance and draws attention to the catalyst stability during the reaction.

Experimental Section

Materials

(Trimethyl)methylcyclopentadienylplatinum(IV) ($(MeCpPtMe_3)$, 99%) and Palladium(II) hexafluoroacetylacetonate ($Pd(hfac)_2$, 95%) were purchased from STREM. Potassium bicarbonate ($KHCO_3$, 99.7%), formaldehyde solution (containing 10–15% methanol as stabilizer, 37 wt.% in H_2O), and Nafion perfluorinated resin solution (5 wt.% in lower aliphatic alcohols and 15–20% water) were purchased from Sigma-Aldrich. Carbon black- Vulcan XC 72R was purchased from the FuelCell store. Glassy carbon rods were purchased from HTW Hochtemperatur-Werkstoffe GmbH (Germany) and used as working electrodes. The electrolyte solution was prepared from ultrapure water (Milli-Q IQ 7000, 18.2 MΩ). All chemicals were received and used without further purification.

Catalyst synthesis

The Pt–Pd bimetallic catalysts with core-shell or alloy structure were synthesized in a vibrated fluidized bed reactor operating at atmospheric pressure, as described elsewhere.[23] We used 0.5 grams of carbon black for each synthesis batch in the reactor. The ALD procedure of Pt deposition[24] and Pd deposition[25] are modified from the reported literature. In summary, the ALD precursors ($MeCpPtMe_3$ and $Pd(hfac)_2$) were kept at 70 °C, and the co-reactants (O_3 and formalin) were kept at room temperature during the experiments. N_2 (99.999 vol%) was used as both carrier and purging gas, and a gas flow of 1 L min^{-1} was used. The reactor was heated and maintained at 200 °C for all ALD process. 1 min dosing of $MeCpPtMe_3$, 5 min dosing of O_3 and 5 min purging were used for Pt ALD cycle. And 12 min dosing of $Pd(hfac)_2$, 6 min dosing of formalin, and 12 min purging were used for Pd ALD cycle. The detailed information on Pt ALD and Pd ALD operation conditions can be found in Table S2. In general, the Pt@Pd core-shell structure catalyst was synthesized by first applying 3 cycles of Pt deposition followed by 12 cycles of Pd deposition with carbon black being fluidized in the reactor. The Pd@Pt core-shell structure catalyst synthesized vice versa, first applied 12 cycles of Pd deposition followed by 3 cycles of Pt deposition. The Pt–Pd alloy structure catalyst was synthesised by first applying 1 cycle of Pt deposition followed by 4 cycles of Pd deposition and repeated the sequence three times to keep the consistency of the Pt–Pd bimetallic catalysts samples. The carbon black powder was pre-treated at 200 °C for 30 minutes under ozone flow and 15 minutes N_2 flow to remove the residual ozone in the samples before each experiment. During all experiments, the carbon black substrate was kept fluidized in the reactor with N_2 flow to achieve homogeneous exposure with precursor and co-reactant.

Material Characterization

The microstructures and particle size distribution of different catalysts were characterized using the JEOL JEM1400 transmission electron microscope (TEM) at a voltage of 120 kV. X-ray diffraction (XRD) measurements were carried out to analyze the crystal structure of the catalysts using a Bruker D2 Phaser instrument. It was operated in powder diffraction mode with Cu Kα radiation at 45 kV and 40 mA. STEM-EDX mapping was conducted to obtain the nanostructure information of the samples before and after the electrochemical tests. It was conducted using the FEI cubed titan Cs-corrected 80–300 kV TEM. Bright Field (BF) images were taken for enhanced contrast using an objective aperture blocking most diffracted electron beams, and elemental mapping in STEM mode was done using the super-X in the ChemiSTEM™ configuration.

Elemental analysis of Pt and Pd was carried out by ICP-OES. Approximately 30 mg of each sample was destructed in 1.5 ml 65% HNO_3 and 4.5 ml 30% HCl using the microwave. The destruction time in the microwave was 60 minutes at 1300 W. After the destruction, the samples were diluted to 50 ml with MQ and analyzed with ICP-OES 8000. X-ray photoelectron spectroscopy (XPS) measurements were carried out using a ThermoFisher Kα system (ThermoFisher Scientific) with a photon energy of 1486.7 eV. Survey scans were conducted using 55 eV pass energy and 0.1 eV per step, and 200 μm spot size with charge neutralization. All peak positions were calibrated according to the C1s peak at 284.8 eV using the CasaXPS software for peak deconvolution.

Electrochemical measurements

The electrochemical reduction of CO_2 was performed in a H-cell setup.[26] The working electrodes were prepared by the drop-casting method. First, the catalyst ink was prepared by adding 4 mg of catalyst, 800 μL deionized water, 150 μL isopropanol, and 50 μL of Nafion perfluorinated resin solution together and sonication for 1 h in the ice bath. Then 30 μL of the catalyst ink was drop cast on the end surface of the glassy carbon rod. The reference electrode used in this paper was Ag/AgCl electrode, and the counter electrode used was Pt foil. A piece of cation-exchange membrane Nafion 117 (FuelCell store) was used to separate the anode and cathode chamber of the H-cell. 0.1 M $KHCO_3$ solution was used as electrolyte on both anode and cathode sides, the cathode chamber was purged by CO_2 for 30 minutes before the experiments. The electrochemical measurements were carried out using a Biologic SP-200 potentiostat (Biologic, France). The applied potential was converted to the reversible hydrogen electrode (RHE) by the formula mentioned in the literature,[27] and the Ohmic loss of the cell was compensated for every experiment. The electrolyte in the cathode chamber was taken out every ten minutes during the testing for analysis by high-performance liquid chromatography (HPLC, Agilent 1260 Infinity).

Acknowledgements

M.L and S.F acknowledge the Ph.D. scholarship provided by the China Scholarship Council (CSC).The authors thank Dr. Damiano La Zara for his help during the project and the constructive ideas he provided.

Conflict of Interest

The authors declare no conflict of interest.

Data Availability Statement

The data that support the findings of this study are available from the corresponding author upon reasonable request.

Keywords: atomic layer deposition · bimetallic electrocatalysts · electrochemical carbon dioxide reduction · core-shell · alloy

[1] R. Kortlever, J. Shen, K. J. Schouten, F. Calle-Vallejo, M. T. Koper, *J. Phys. Chem. Lett.* **2015**, *6*, 4073–4082.
[2] C. Chen, J. F. Khosrowabadi Kotyk, S. W. Sheehan, *Chem* **2018**, *4*, 2571–2586.
[3] J. M. Spurgeon, B. Kumar, *Energy Environ. Sci.* **2018**, *11*, 1536–1551.
[4] a) D. Pavesi, F. S. M. Ali, D. Anastasiadou, T. Kallio, M. Figueiredo, G.-J. M. Gruter, M. T. M. Koper, K. J. P. Schouten, *Catal. Sci. Technol.* **2020**, *10*, 4264–4270; b) K. Van Daele, B. De Mot, M. Pupo, N. Daems, D. Pant, R. Kortlever, T. Breugelmans, *ACS Energy Lett.* **2021**, *6*, 4317–4327; c) C. Zhao, J. Wang, J. B. Goodenough, *Electrochem. Commun.* **2016**, *65*, 9–13.
[5] C. Vogt, E. Groeneveld, G. Kamsma, M. Nachtegaal, L. Lu, C. J. Kiely, P. H. Berben, F. Meirer, B. M. Weckhuysen, *Nat. Catal.* **2018**, *1*, 127–134.
[6] a) B. J. O'Neill, D. H. K. Jackson, J. Lee, C. Canlas, P. C. Stair, C. L. Marshall, J. W. Elam, T. F. Kuech, J. A. Dumesic, G. W. Huber, *ACS Catal.* **2015**, *5*, 1804–1825; b) J. A. Singh, N. Yang, S. F. Bent, *Annu. Rev. Chem. Biomol. Eng.* **2017**, *8*, 41–62.
[7] C. Zhao, J. Wang, *Chem. Eng. J.* **2016**, *293*, 161–170.
[8] Y. Hori, H. Wakebe, T. Tsukamoto, O. Koga, *Electrochim. Acta* **1993**.
[9] X. Min, M. W. Kanan, *J. Am. Chem. Soc.* **2015**, *137*, 4701–4708.
[10] S. Chatterjee, C. Griego, J. L. Hart, Y. Li, M. L. Taheri, J. Keith, J. D. Snyder, *ACS Catal.* **2019**, *9*, 5290–5301.
[11] R. Kortlever, I. Peters, S. Koper, M. T. M. Koper, *ACS Catal.* **2015**, *5*, 3916–3923.
[12] M. T. M. Koper, *J. Electroanal. Chem.* **2011**, *660*, 254–260.
[13] R. Kortlever, C. Balemans, Y. Kwon, M. T. M. Koper, *Catal. Today* **2015**, *244*, 58–62.
[14] H. Van Bui, F. Grillo, J. R. van Ommen, *Chem. Commun.* **2016**, *53*, 45–71.
[15] R. Beetstra, U. Lafont, J. Nijenhuis, E. M. Kelder, J. R. van Ommen, *Chem. Vap. Deposition* **2009**, *15*, 227–233.
[16] X. Liang, L. B. Lyon, Y.-B. Jiang, A. W. Weimer, *J. Nanopart. Res.* **2012**, *14*.
[17] A. De, J. Datta, I. Haldar, M. Biswas, *ACS Appl. Mater. Interfaces* **2016**, *8*, 28574–28584.
[18] E. I. Vovk, A. V. Kalinkin, M. Y. Smirnov, I. O. Klembovskii, V. I. Bukhtiyarov, *J. Phys. Chem. C* **2017**, *121*, 17297–17304.
[19] A. B. M. Brun, J. C. Bertolini, *J. Electron Spectrosc. Relat. Phenom.* **1998**, *104*, 55–60.
[20] a) N. V. Long, T. Duy Hien, T. Asaka, M. Ohtaki, M. Nogami, *Int. J. Hydrogen Energy* **2011**, *36*, 8478–8491; b) E. J. Jang, J. Lee, D. G. Oh, J. H. Kwak, *ACS Catal.* **2021**, *11*, 5894–5905.
[21] J. S. Diercks, M. Georgi, J. Herranz, N. Diklić, P. Chauhan, A. H. Clark, R. Hübner, A. Faisnel, Q. Chen, M. Nachtegaal, A. Eychmüller, T. J. Schmidt, *ACS Appl. Energ. Mater.* **2022**, *5*, 8460–8471.
[22] J. Hong, K. T. Park, Y. E. Kim, D. Tan, Y. E. Jeon, J. E. Park, M. H. Youn, S. K. Jeong, J. Park, Y. N. Ko, W. Lee, *Chem. Eng. J.* **2022**, *431*.
[23] a) D. Zhang, D. La Zara, M. J. Quayle, G. Petersson, J. R. van Ommen, S. Folestad, *ACS Appl. Bio Mater.* **2019**, *2*, 1518–1530; b) D. Zhang, M. J. Quayle, G. Petersson, J. R. van Ommen, S. Folestad, *Nanoscale* **2017**, *9*, 11410–11417.
[24] F. Grillo, H. Van Bui, J. A. Moulijn, M. T. Kreutzer, J. R. van Ommen, *J. Phys. Chem. Lett.* **2017**, *8*, 975–983.
[25] J. W. Elam, A. Zinovev, C. Y. Han, H. H. Wang, U. Welp, J. N. Hryn, M. J. Pellin, *Thin Solid Films* **2006**, *515*, 1664–1673.
[26] Y. Song, P. N. Pintauro *J. Appl. Electrochem.* **1990**, *21*, 21–27.
[27] L. Wang, C.-Y. Lee, P. Schmuki, *J. Mater. Chem. A* **2013**, *1*, 212–215.

Manuscript received: July 28, 2022
Revised manuscript received: October 21, 2022
Accepted manuscript online: October 24, 2022
Version of record online: ■■, ■■■

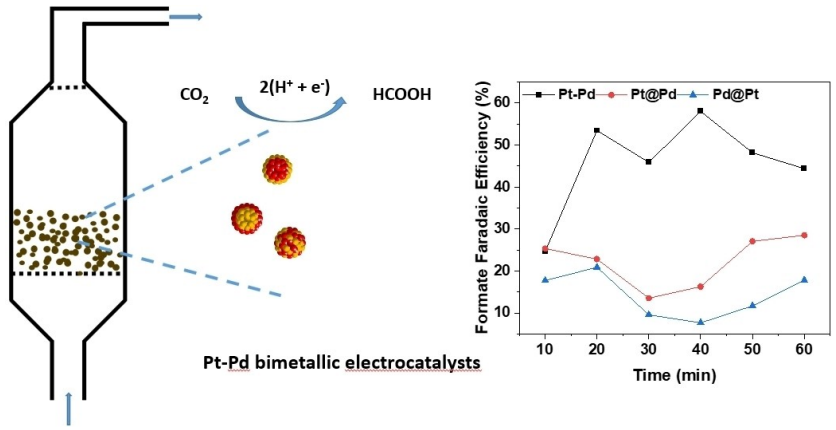

M. Li, S. Fu, Dr. S. Saedy, A. Rajendrakumar, Dr. F. D. Tichelaar, Dr. R. Kortlever*, Prof. J. R. van Ommen*

1 – 8

Nanostructuring Pt-Pd Bimetallic Electrocatalysts for CO_2 Reduction Using Atmospheric Pressure Atomic Layer Deposition

This study demonstrates a way of synthesizing well-controlled **core-shell** and **alloy catalysts by ALD** on the surface of the powder substrate material. Pt–Pd bimetallic catalysts have been synthesized and used for the **CO_2 electro-reduction reaction**. The effect of nanostructuring on bimetallic catalysts' selectivity was investigated.